BIOCHEMISTRY
including biophysical chemistry & molecular biology
Article

Biochemistry **2010,** *49,* 645–652 645
DOI: 10.1021/bi901874e

Measurement of Intrinsic Rate Constants in the Tyrosine Hydroxylase Reaction†

Bekir E. Eser‡ and Paul F. Fitzpatrick*,§

‡*Department of Chemistry, Texas A&M University, College Station, Texas 77843 and* §*Department of Biochemistry and Center for Biomedical Neuroscience, University of Texas Health Science Center, San Antonio, Texas 78229*

Received November 2, 2009; Revised Manuscript Received December 17, 2009

ABSTRACT: Tyrosine hydroxylase (TyrH) is a pterin-dependent mononuclear non-heme aromatic amino acid hydroxylase that catalyzes the conversion of tyrosine to dihydroxyphenylalanine (DOPA). Chemical quench analyses of the enzymatic reaction show a burst of DOPA formation, followed by a linear rate equal to the k_{cat} value at both 5 and 30 °C. The effects of increasing solvent viscosity confirm that k_{cat} is ~84% limited by diffusion, most probably due to slow product release, and that tyrosine has a commitment to catalysis of 0.45. The effect of viscosity on the k_{cat}/K_m for 6-methyltetrahydropterin is greater than the theoretical limit, consistent with the coupling of pterin binding to the movement of a surface loop. The absorbance changes in the spectrum of the tetrahydropterin during the first turnover, the kinetics of DOPA formation during the first turnover, and the previously described kinetics for formation and decay of the Fe(IV)O intermediate [Eser, B. E., Barr, E. W., Frantom, P. A., Saleh, L., Bollinger, J. M., Jr., Krebs, C., and Fitzpatrick, P. F. (2007) *J. Am. Chem. Soc. 129*, 11334−11335] were analyzed globally, yielding a single set of rate constants for the TyrH reaction. Reversible binding of oxygen is followed by formation of Fe(IV)O and 4a-hydroxypterin with a rate constant of 13 s^{-1} at 5 °C. Transfer of oxygen from Fe(IV)O to tyrosine to form DOPA follows with a rate constant of 22 s^{-1}. Release of DOPA and/or the 4a-hydroxypterin with a rate constant of 0.86 s^{-1} completes the turnover.

Tyrosine hydroxylase (TyrH)[1] is a member of the pterin-dependent aromatic amino acid hydroxylase family (*1*, *2*); these enzymes utilize a mononuclear non-heme iron and a reduced pterin to activate molecular oxygen for the hydroxylation of their corresponding amino acid substrates. TyrH, which is found in the brain and adrenal gland, catalyzes conversion of L-tyrosine to L-dihydroxyphenylalanine (DOPA) (Scheme 1). This is the first and rate-limiting step in the biosynthesis of the catecholamine neurotransmitters dopamine, noradrenaline, and adrenaline. A deficiency of TyrH is associated with several neurological disorders, including DOPA-responsive Parkinson's disease, progressive encephalopathy, DOPA-nonresponsive dystonia, and DOPA-responsive dystonia (Segawa's disease) (*3*, *4*). The other members of the family are also physiologically significant; phenylalanine hydroxylase, a liver enzyme, catalyzes the conversion of phenylalanine in the diet to tyrosine, and tryptophan hydroxylase, a brain enzyme, converts tryptophan to 5-hydroxytryptophan as a precursor to the neurotransmitter serotonin.

The members of the aromatic amino acid hydroxylase family have similar active sites in which the iron atom is coordinated by the common 2-His-1-Glu facial triad motif (*5*, *6*). Studies of the three enzymes have established that they share a common catalytic mechanism (*7*−*12*), shown for TyrH in Scheme 2 (*1*). The cationic amino acid intermediate in Scheme 2 was originally proposed on the basis of an analysis of the kinetics of TyrH with a series of para-substituted phenylalanines (*8*). Subsequent measurements of the secondary deuterium kinetic isotope effect on hydroxylation for all the aromatic amino acid hydroxylases provided further evidence of an electrophilic aromatic substitution reaction mechanism (*7*, *9*, *11*, *12*). Initial indirect evidence for the Fe(IV)O intermediate came from the observation that the 4a-HO-6MPH$_3$ product could be formed in the absence of amino acid hydroxylation, establishing that heterolytic cleavage of the oxygen−oxygen bond is required to form the hydroxylating intermediate (*7*, *13*, *14*). This set the formal oxidation level of the hydroxylating intermediate as Fe(IV)O in the absence of additional electron transfer steps. More recently, rapid freeze quench Mössbauer spectroscopy provided direct evidence of an Fe(IV) species as the hydroxylating intermediate in the TyrH reaction (*15*). The initial iron−peroxo−pterin intermediate in Scheme 2 has not been detected, although E332A TyrH produces a pterin species with a UV absorbance spectrum consistent with a 4a-hydroperoxypterin (*16*). Together these results have provided strong evidence of the intermediates in the mechanism of Scheme 2. Still, a complete understanding of the reaction of TyrH requires knowledge of the rate constants for their interconversion. The experiments described here were designed to determine such rate constants.

EXPERIMENTAL PROCEDURES

Chemicals. 6-Methyltetrahydropterin was from Schircks Laboratories (Jona, Switzerland). Ferrous ammonium sulfate, Hepes, sucrose, and trehalose were purchased from Fisher (Pittsburgh, PA). Glycerol and tyrosine were from Sigma-Aldrich (Milwaukee, WI). The GEMINI reverse-phase C18 HPLC

†This work was supported by in parts by grants from the National Institutes of Health (R01 GM047291) and The Welch Foundation (AQ-1245).

*To whom correspondence should be addressed: Department of Biochemistry, University of Texas Health Science Center, San Antonio, TX 78229. E-mail: fitzpatrick@biochem.uthscsa.edu. Phone: (210) 567-8264. Fax: (210) 567-8778.

[1]Abbreviations: TyrH, tyrosine hydroxylase; DOPA, dihydroxyphenylalanine; 6MPH$_4$, 6-methyltetrahydropterin; 4a-HO-6MPH$_3$, 4a-hydroxypterin; DOPA, 3,4-dihydroxyphenylalanine.

Published on Web 12/21/2009

column was obtained from Phenomenex (Torrance, CA). All other reagents were of the highest purity commercially available.

Expression and Purification of TyrH. Rat TyrH was expressed in *Escherichia coli* and purified as previously described (*17*, *18*), with the exceptions that cell cultures were grown in LB broth containing 500 μM $FeCl_3$ and 2 mM $MgSO_4$ and growth continued for ~20 h at 20 °C after induction with isopropyl β-thiogalactoside. To remove the ferric iron present in the enzyme as purified, enzyme to be used in the rapid reaction analyses was dissolved in 200 mM Hepes (pH 7.5), 10% glycerol, and 0.1 M KCl containing 5 mM EDTA and incubated for 1 h on ice before being dialyzed against the same buffer without EDTA. The iron content was determined using a Perkin-Elmer Analyst 700 atomic absorption spectrophotometer (*19*). For experiments in which viscogen was used, the enzyme was dialyzed into buffer that contained no glycerol [200 mM Hepes (pH 7.5) and 0.1 M KCl].

Steady-State Kinetics. Steady-state kinetic parameters of TyrH were determined using a colorimetric end point assay to measure DOPA production, as previously described (*20*). Conditions were 0.1−0.5 μM TyrH, 100 μg/mL catalase, 1 mM dithiothreitol (DTT), 10 μM ferrous ammonium sulfate, and either 1 mM $6MPH_4$ when tyrosine was the varied substrate (3−300 μM) or 200 μM tyrosine when $6MPH_4$ was the varied substrate (5 μM to 1 mM). The buffer consisted of 200 mM Hepes (pH 7.5) and 0.1 M KCl, with or without viscogen. The absolute viscosities (η) for buffers at 5 and 30 °C were calculated using values reported in the literature (*21*−*23*). The small effects of buffer and salt on the viscosity of the solutions were neglected.

Chemical Quench. Chemical quench experiments were performed using an SFM-400/Q rapid-mixing instrument from Bio-Logic (Claix, France) in quenched-flow mode. The instrument was made anaerobic through incubation with a sodium dithionite solution (~100 mM) for at least 2 h. The water bath was bubbled with nitrogen gas to prevent diffusion of O_2 into the system. Apo-TyrH (30−40 μM) in 200 mM Hepes (pH 7.5), 10% glycerol, and 0.1 M KCl (total volume of ~10 mL) was made anaerobic in a tonometer through at least 20 argon−vacuum cycles. Ferrous ammonium sulfate (~20 μL, ~0.9 equiv of enzyme) was then added to the tonometer under argon. The $6MPH_4$ stock solution (~40 mM) was prepared in 2 mM HCl; an extinction coefficient of 17.8 mM^{-1} cm^{-1} in 2 M perchloric acid was used to determine the exact concentration. A volume corresponding to a final concentration in the tonometer of 2 mM $6MPH_4$ was placed in the side arm under argon. Additional argon−vacuum cycles were performed prior to the $6MPH_4$ solution being mixed with the tonometer contents, which were then loaded into one of the syringes of the rapid-mixing instrument. A second syringe was loaded with buffer containing 500 μM tyrosine that had been bubbled with pure oxygen gas for at least 20 min. This was done either on ice to produce an oxygen concentration of 1.9 mM or at room temperature to produce a concentration of 1.2 mM. The quenching solution, 5 M HCl, was loaded into a third syringe. The tonometer contents were mixed with the tyrosine-containing oxygenated buffer and quenched with acid after being aged through a 90 μL (N° 3) delay line. Tyrosine and DOPA were separated on a Phenomenex C18 HPLC column (250 mm × 4.6 mm) with an isocratic mobile phase of 15 mM sodium phosphate (pH 7.0) at a flow rate of 1 mL/min. The amount of DOPA was quantified using a Waters 2475 Multi λ fluorescence detector with an excitation wavelength of 270 nm and an emission wavelength of 310 nm.

Scheme 1

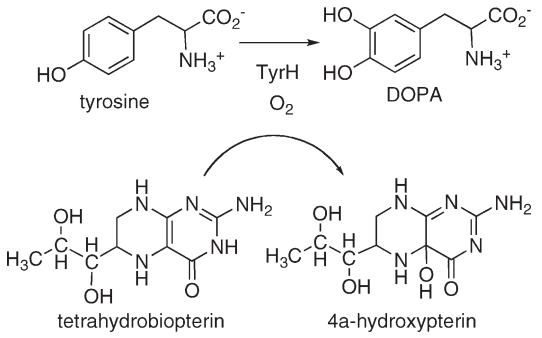

Scheme 2

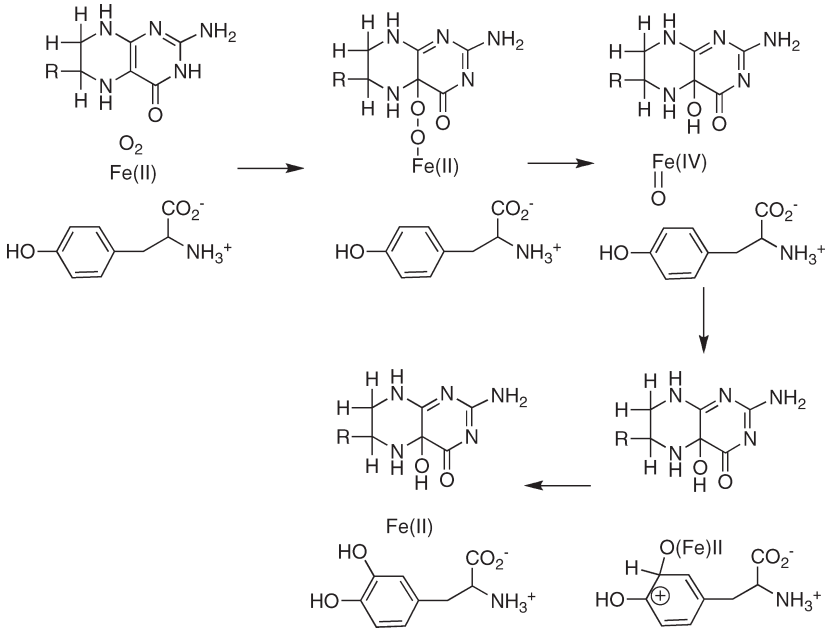

Stopped-Flow Spectrophotometry. Single-turnover kinetics of TyrH were monitored using an Applied Photophysics (Leatherhead, U.K.) SX20 stopped-flow spectrophotometer in absorbance mode. The instrument was made anaerobic in the same way as described above for the chemical quench experiment. A solution of apo-TyrH (200 μM) and tyrosine (550 μM) in 200 mM Hepes (pH 7.5) and 0.1 M KCl was made anaerobic in a tonometer through at least 20 argon−vacuum cycles. A stoichiometric amount of ferrous ammonium sulfate (~20 μL, ~0.9 equiv of enzyme) was then added to the tonometer under argon. A $6MPH_4$ solution, corresponding to a final concentration of 1.1 mM, was placed in the side arm of the tonometer under argon. Additional argon−vacuum cycles were performed before the $6MPH_4$ solution was mixed with the tonometer contents. The tonometer was then loaded into one of the syringes of the stopped-flow instrument. The second syringe was loaded with the same buffer containing 120 μM oxygen at 5 °C.

Data Analysis. The kinetics of DOPA formation from the chemical quench experiments were analyzed using the global analysis program KinTek Explorer Pro, which utilizes direct numerical integration to simulate experimental results (KinTek Corp., Austin, TX) (*24*). SpecFit (*25*, *26*) (Spectrum Software Associates) was used for initial analysis of stopped-flow data at multiple wavelengths by singular-value decomposition. Subsequent global analyses were conducted with KinTek Explorer. Error analysis was done with the FitSpace Explorer option of KinTek Explorer (*27*) and a threshold value of 1.2 sum square error (SSE). Igor Pro (Wavemetrics, Lake Oswego, OR) was used for analysis of the effects of viscosity on the steady-state kinetics using eqs 1−3.

RESULTS

Chemical Quench Experiments. The kinetics of DOPA formation during the first few turnovers of the TyrH reaction were analyzed by chemical quench methods. To do so, the anaerobic complex of ferrous TyrH (30−40 μM) with $6MPH_4$ (2.0 mM) was mixed with an equal volume of buffer containing tyrosine (500 μM) and O_2 (1.9 mM at 5 °C and 1.2 mM at 30 °C). The tyrosine, oxygen, and $6MPH_4$ concentrations were set sufficiently high to achieve complete and rapid binding (> $15K_m$). The reaction was quenched with 5 M HCl at times from 10 ms to several seconds, and the samples were analyzed by HPLC to quantify the amount of the product DOPA. The time courses at 5 and 30 °C are shown in Figure 1. An initial burst can be clearly seen at both temperatures. For quantitative analysis, the data were fit to the mechanism in Scheme 3 using KinTek Explorer; here k_{burst} represents the rate constant for the formation of DOPA during the first turnover, and k_{linear} represents the rate of DOPA formation during subsequent turnovers and should match k_{cat}. Binding of substrates was assumed to be rapid and was not included in the analysis. The data at 5 °C could be fit with rate constants of 7.0 ± 2.4 s^{-1} for the burst phase and 0.65 ± 0.05 s^{-1} for the linear phase. The fit of the data at 30 °C yields values for k_{burst} and k_{linear} of 18.8 ± 5.4 and 3.5 ± 0.5 s^{-1}, respectively.

Steady-State Viscosity Experiments. The chemical quench analyses establish that the chemical steps in the TyrH reaction that result in DOPA formation are significantly faster than the following steps. These slower steps are frequently product release or conformational changes associated with product release (*28*−*35*). Product release should be diffusion-limited, with a rate constant dependent on the viscosity of the medium (*33*).

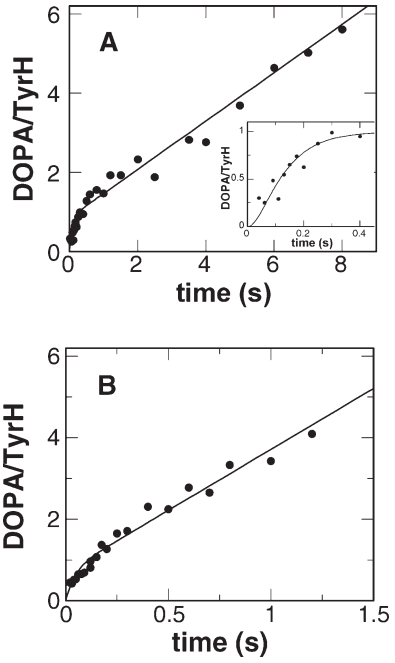

FIGURE 1: Time course at (A) 5 or (B) 30 °C for the formation of DOPA from the reaction of TyrH (30−40 μM) and $6MPH_4$ (2 mM) with an equal volume of Tyr (500 μM) and O_2 (1.9 mM at 5 °C and 1.2 mM at 30 °C). The lines are from fits to the mechanism in Scheme 3 with values for k_{burst} (pseudo-first-order rate constant with respect to oxygen concentration) and k_{linear} of 7.0 ± 2.4 and 0.65 ± 0.05 s^{-1}, respectively, for the data at 5 °C and of 18.8 ± 5.4 and 3.5 ± 0.5 s^{-1}, respectively, for the data at 30 °C. The line in the inset of panel A is based on the mechanism in Scheme 4, with the rate constants listed in Table 2.

Consequently, the extent to which product release limits turnover will be reflected in the sensitivity of the k_{cat} value to the viscosity of the medium. Entry of the substrate into the active site is similarly expected to be diffusion-limited, so that the effects of viscosity on k_{cat}/K_m values will reflect the magnitude of the rate constant for the initial binding relative to those for subsequent steps up to and including the first irreversible step (*30*−*33*, *35*).

Glycerol, sucrose, and trehalose were used as viscogens to determine the effect of solvent viscosity on the steady-state kinetic parameters for TyrH. However, in initial experiments, the effects of glycerol were nonlinear and suggested that glycerol directly inhibited the enzyme at high concentrations. In fact, PheH has been reported to be inhibited by glycerol (*36*). Therefore, more complete analyses were conducted with only sucrose and trehalose as viscogens.

The effects of sucrose and trehalose on the steady-state kinetic parameters for TyrH are illustrated in Figures 2−4. The data are plotted as the ratio of the relevant kinetic parameter in the absence of viscogen to that in its presence as a function of the relative viscosity of the solvent. The effect of viscosity is the slope of such a plot and can take values between 0 and 1. A viscosity effect of 0 means the rate of the reaction is completely independent of solvent viscosity, whereas an effect of 1 indicates a completely diffusion-limited event. To analyze the data, the initial rates as a function of substrate concentration at each concentration of viscogen were fit to eq 1 to yield the viscosity effects on both k_{cat} and k_{cat}/K_m simultaneously

$$v = \frac{k_{cat}S}{K_m[1 + m(\mu)] + S[1 + n(\mu)]} \quad (1)$$

Scheme 3

$$\text{TyrH:Fe(II)} + \text{Tyr} + 6\text{MPH}_4 + \text{O}_2 \xrightarrow{k_{burst}} \text{TyrH:Fe(II):DOPA:4a-HO-6MPH}_3$$

$$\text{TyrH:Fe(II):DOPA:4a-HO-6MPH}_3 \xrightarrow{k_{linear}} \text{TyrH:Fe(II)} + \text{DOPA} + \text{4a-HO-6MPH}_3$$

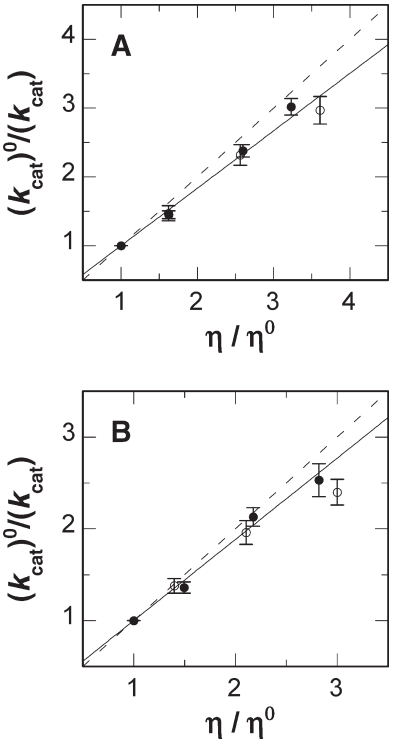

FIGURE 2: Effect of solvent viscosity on the k_{cat} value at (A) 5 and (B) 30 °C for sucrose (●) or trehalose (○) as the viscogen. The solid lines are based on the averages of the viscosity effects at each temperature for sucrose and trehalose determined from eq 1. The dashed lines show the theoretical limits for a completely diffusion limited reaction.

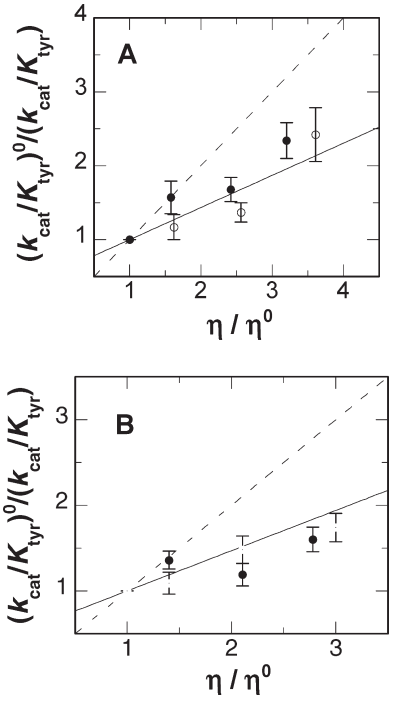

FIGURE 3: Effect of solvent viscosity on the k_{cat}/K_m value for tyrosine at (A) 5 and (B) 30 °C for sucrose (●) or trehalose (○) as the viscogen. The solid lines are based on the averages of the viscosity effects at each temperature for sucrose and trehalose determined from eq 2 (A) or eq 1 (B). The dashed lines show the theoretical limits for a completely diffusion limited reaction.

where μ is the relative viscosity $(\eta/\eta^0)^2$ minus 1 and m and n are the viscosity effects on k_{cat}/K_m and k_{cat}, respectively. Equation 2 was used instead of eq 1 to calculate the viscosity effects on the k_{cat}/K_m value for tyrosine at 5 °C, using only the initial rate data obtained at low tyrosine concentrations.

$$v = \frac{k_{cat}S}{K_m[1 + m(\mu)]} \quad (2)$$

The results are summarized in Table 1.

Increasing the viscosity of the solution with either sucrose or trehalose results in a significant decrease in the k_{cat} value at both 5 and 30 °C (Table 1 and Figure 2). The effect at both temperatures is independent of the identity of the viscogen, with an average effect of 0.84 at 5 °C and 0.88 at 30 °C. This indicates that the k_{cat} value is significantly limited by a diffusional event. Sucrose and trehalose also have similar effects on the k_{cat}/K_m value for tyrosine at both 5 and 30 °C, with average values of 0.44 and 0.42 at the two temperatures (Figure 3). The values suggest that the k_{cat}/K_m value for tyrosine is ~45% limited by diffusion of tyrosine into the active site. The effects of increased viscosity on the k_{cat}/K_m value for $6MPH_4$ are more complex. The effect varies with both the temperature and identity of the viscogen (Figure 4 and Table 1). For both sucrose and trehalose, the effect on k_{cat}/K_{6MPH_4} is much greater at 30 °C than at 5 °C. Only at 5 °C is the viscosity effect within the expected range of 0−1. In all the other cases, the viscosity effect is greater than 1 (Figure 4B and Table 1). Such deviations from the expected limit have previously been attributed to internal motions in proteins occurring concomitantly with binding (*28*, *37*−*39*).

Single-Turnover Stopped-Flow Experiments. As a complementary approach to determining rate constants for individual steps in the TyrH reaction, stopped-flow absorbance spectroscopy was used to monitor the pterin intermediates that form during the reaction of TyrH. The non-heme iron center of TyrH is colorless, although there is a weak charge transfer absorbance band in the near UV (*19*), ruling out the possibility of monitoring the reaction by following changes in the absorbance spectrum of the iron. However, several oxidized and reduced forms of pterin have distinct absorbance spectra at 200−450 nm (*7*). An anaerobic TyrH (200 μM)/$6MPH_4$ (1.1 mM)/Tyr (550 μM) solution was mixed with an equal volume of oxygenated buffer (120 μM) at 5 °C. Under these conditions, the concentration of oxygen limits the reaction to a single turnover. Figure 5 shows the resulting absorbance changes at 246 and 318 nm. The 4a-hydroxypterin product absorbs maximally at 246 nm, while the absorbance changes at 318 nm reflect both the formation of the hydroxypterin product and its subsequent dehydration to quinonoid dihydropterin (*7*). The absorbance traces at both wavelengths were fit simultaneously to

[2]Parameters denoted with a superscript zero, such as k_{cat}^0 or η^0, refer to the values in the absence of viscogen.

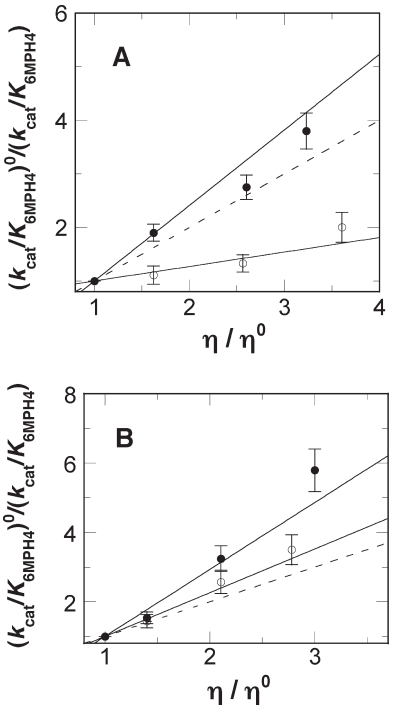

FIGURE 4: Effect of solvent viscosity on the k_{cat}/K_m value for $6MPH_4$ at (A) 5 and (B) 30 °C for sucrose (●) or trehalose (○) as the viscogen. The solid lines are linear regression fits with slopes corresponding to the viscosity effects reported in Table 1. The dashed lines show the theoretical limits for a completely diffusion limited reaction.

various sequential mechanisms using SpecFit (*25*, *26*). A three-step sequential mechanism, with rate constants of 15, 0.7, and 0.024 s^{-1} accounted well for the data at both wavelengths. This analysis provided estimates of the rate constants for formation of the bound hydroxypterin from the reaction of oxygen with the enzyme complex, for a subsequent step that resulted in a further spectral change, and for the slow dehydration of the hydroxypterin to the quinonoid dihydropterin.

Global Analyses. The stopped-flow results in Figure 5 provide estimates of the rate constants for steps in which the absorbance of the pterin substrate changes significantly. The chemical quench experiments in Figure 1 provide rate constants for hydroxylation of the amino acid substrate and for k_{cat}. The earlier freeze quench Mössbauer data (*15*) provide rate constants for formation and decay of the Fe(IV) intermediate. To integrate the results of the three analyses into a single kinetic mechanism, global analysis was conducted using all the single-turnover data at 5 °C. The data from all the experiments were fit simultaneously to the mechanism in Scheme 4 using KinTek Explorer Pro (KinTek Corp.) (*24*). Scheme 4 describes a minimal mechanism of four steps plus a fifth step to account for the hydrolysis of the 4a-HO-$6MPH_3$ product. It was necessary to include an initial step for oxygen binding because the individual experiments were conducted at different concentrations of oxygen. We have previously analyzed the oxygen dependence of the absorbance changes that occur upon oxygen binding (*16*); the rate constants for the reversible oxygen binding step (k_1 and k_{-1}) from that study were used for our global analysis. The rate constant of 0.024 s^{-1} obtained from the final decrease in absorbance at 246 nm and increase at 318 nm in the stopped-flow experiment is consistent with reported values for nonenzymatic dehydration of a 4a-hydroxypterin to give quinonoid dihydropterin in solution (*7*, *13*, *40*, *41*), so that this rate constant was not varied in the

Table 1: Effects of Viscosity on the Steady-State Kinetic Parameters for TyrH[a]

viscogen	temp (°C)	k_{cat}[b]	k_{cat}/K_{tyr}[c]	k_{cat}/K_{6MPH_4}[b]
sucrose	5	0.89 ± 0.09	0.49 ± 0.09	1.41 ± 0.26
trehalose	5	0.78 ± 0.07	0.38 ± 0.10	0.27 ± 0.10
sucrose	30	0.83 ± 0.03	0.30 ± 0.11	1.93 ± 0.27
trehalose	30	0.94 ± 0.10	0.54 ± 0.15	1.26 ± 0.29

[a]Conditions: 0.1−0.5 μM TyrH, 100 μg/mL catalase, 1 mM DTT, 10 μM ferrous ammonium sulfate, 200 mM Hepes (pH 7.5), and 0.1 M KCl. [b]With 200 μM tyrosine with varied concentrations of $6MPH_4$ (5 μM to 1 mM). [c]With 1 mM $6MPH_4$ with varied concentrations of tyrosine (3−300 μM).

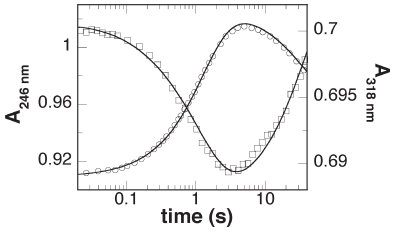

FIGURE 5: Stopped-flow absorbance traces at 246 (○) and 318 nm (□) for the reaction of a 100 μM TyrH/Fe(II)/$6MPH_4$/Tyr solution with 60 μM O_2. The solid lines were calculated from the mechanism in Scheme 4 using the rate constants and extinction coefficients listed in Table 2.

global analysis. Estimates for the extinction coefficients of free $6MPH_4$ and 4a-HO$6MPH_3$ were also taken from previous studies (*7*, *16*). To obtain estimates of the extinction changes for enzyme-bound pterin species and of the concentrations of active enzyme, these values were adjusted manually by taking advantage of the live simulation display option of KinTek Explorer (*24*). The resulting fraction of active enzyme was at least 95%, except for the freeze quench Mössbauer data, where the fraction of active enzyme concentration was 80% (*16*). Finally, a global fit to all three data sets was conducted to yield values of k_2, k_3, and k_4. The confidence intervals for the resulting values were determined using the FitSpace Explorer option of KinTek Explorer (*27*). FitSpace determines estimates of the confidence intervals of fitted parameters by determining the dependence of the sum square error (SSE) on each pair of parameters while allowing all other parameters to be varied (*27*). The best-fit values for the fitted rate constants, their confidence intervals (lower and upper boundaries), and extinction coefficients from the global fitting analysis are listed in Table 2. The values of k_2, k_4, and k_5 agree well with the results of analyzing the stopped-flow data alone. The value of k_4 agrees well with k_{cat}, consistent with slow product release, while the value of k_{burst} is within error of the net rate constant for the first three steps, consistent with hydroxylation occurring with rate constant k_3. Analysis of the Mössbauer data alone previously gave rate constants for formation and decay of the Fe(IV) species comparable to the values of k_2 and k_3. To illustrate the agreement between the data and the kinetic model, the data in Table 2 were used to generate the lines in Figures 5 and 6 and in the inset of Figure 1A.

DISCUSSION

Because TyrH and the other aromatic amino acid hydroxylases lack a chromophoric cofactor, measurement of individual rate constants poses a significant challenge. However, individual

Scheme 4

$$\text{TyrH:Fe(II):Tyr:6MPH}_4 + \text{O}_2 \underset{k_{-1}}{\overset{k_1}{\rightleftharpoons}} \text{TyrH:Fe(II):Tyr:6MPH}_4\text{:O}_2$$

$$\text{TyrH:Fe(II):Tyr:6MPH}_4\text{:O}_2 \xrightarrow{k_2} \text{TyrH:Fe(IV)O:Tyr:4a-HO-6MPH}_3$$

$$\text{TyrH:Fe(IV)O:Tyr:4a-HO-6MPH}_3 \xrightarrow{k_3} \text{TyrH:Fe(II):DOPA:4a-HO-6MPH}_3$$

$$\text{TyrH:Fe(II):DOPA:4a-HO-6MPH}_3 \xrightarrow{k_4} \text{TyrH:Fe(II)} + \text{4a-HO-6MPH}_3 + \text{DOPA}$$

$$\text{4a-HO-6MPH}_3 \xrightarrow{k_5} \text{q-6MPH}_2$$

Table 2: Values of the Rate Constants, Their Confidence Intervals, and Associated Extinction Changes Obtained from Global Fitting of the Data in Figures 1A and 5 and the Mössbauer Time Course from ref *15*, All at 5 °C

rate constant	best-fit value	lower bound	upper bound	$\Delta\varepsilon_{246}$ (mM^{-1} cm^{-1})	$\Delta\varepsilon_{318}$ (mM^{-1} cm^{-1})
k_1	300 mM^{-1} s^{-1}[a]	–	–	–	–
k_{-1}	50 s^{-1}[a]	–	–	–	–
k_2	12.7 s^{-1}	9.3 s^{-1}	17.7 s^{-1}	2.0	−0.4
k_3	22.5 s^{-1}	14.4 s^{-1}	44.0 s^{-1}	–	–
k_4	0.86 s^{-1}	0.54 s^{-1}	1.55 s^{-1}	8.0	−0.7
k_5	0.024 s^{-1}[b]	–	–	−6.0	1.5

[a]Taken from ref *16* and kept fixed. [b]Determined from the stopped-flow data alone and kept fixed.

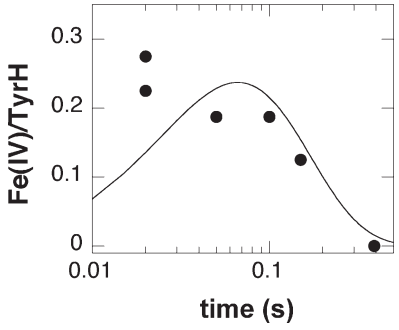

FIGURE 6: Comparison of predicted concentrations of the Fe(IV)O intermediate with the experimentally determined concentrations. The line was calculated from the mechanism of Scheme 4 with the rate constants in Table 2. The points are taken from ref *15*.

rapid quench analyses of the Fe(IV) intermediate and the amino acid product and stopped-flow spectroscopic analyses of changes in the spectrum of the pterin substrate each allow measurement of a subset of the rate constants in Scheme 4, and the combination of results from the different approaches means the values for the rate constants of interest, k_2, k_3, and k_4, are all based on more than one experimental approach. The global analysis described here of the results from separate, chemical quench, freeze quench, and stopped-flow experiments yields values of these rate constants consistent with all the data. The first step in Scheme 4 is reversible binding of oxygen, with no detectable absorbance change upon oxygen binding. The rate constants for this step were determined previously by analyzing the effect of the oxygen concentration on the absorbance changes in stopped-flow analyses (*16*). The second step corresponds to an increase in absorbance at 246 nm and a decrease at 318 nm as the 4a-hydroxypterin forms. In the mechanism of Scheme 2, formation of the 4a-hydroxypterin accompanies formation of Fe(IV)O. This is confirmed by the Mössbauer time course, although the rapid quench Mössbauer data in the first 30 ms do not themselves allow reliable estimation of the value of k_2. While Mössbauer spectroscopy is the most direct measure of the Fe(IV)O intermediate, it is also the least precise. Such analyses are expensive in spectrometer time and enzyme, limiting the number of data points, and it is not possible to freeze the reaction rapidly enough on the millisecond time scale to obtain high accuracy at these early time points. Still, these data show directly at what times the Fe(IV) intermediate is present, placing important constraints on the rate constants for its formation and decay. The next step is hydroxylation of the amino acid by the Fe(IV)O with rate constant k_3. This step does not correspond to a change in the absorbance spectrum of the pterin bound to the enzyme. However, the chemical quench analysis of DOPA formation establishes that DOPA is formed in this step, and the freeze quench Mössbauer experiment establishes that Fe(IV)O decays in this step. The fourth step is assigned to product release on the basis of the agreement of k_4 with k_{cat} and the conclusion from both the viscosity effects and the chemical quench analysis that product release limits turnover. The final step with rate constant k_5 is required to account for the absorbance changes seen in the stopped-flow experiment at longer times. This is a nonenzymatic step; the rate constant for k_5 in Table 2 agrees well with previous analyses.

The absorbance changes for the second step in Scheme 4 are less than expected for the formation of 4a-hydroxypterin at neutral pH (*7*). However, the sum of the absorbance changes for the second and fourth steps at both 246 and 318 nm is consistent with the overall formation of 4a-hydroxypterin from $6MPH_4$. This suggests that the spectrum of 4a-hydroxypterin within the enzyme active site is perturbed. Only upon release of the pterin from the enzyme is the typical absorbance spectrum of a 4a-hydroxypterin seen. The agreement of k_4 with the rate constant for the linear rate of the chemical quench analysis and the k_{cat} value establishes this as the rate constant for product

Table 3: Values of Association Rate Constants and Forward Commitments for Tyrosine Binding Calculated from the Effects of Viscosity on k_{cat}/K_{tyr}

temp (°C)	k_{on} (μM^{-1} s^{-1})	k_f/k_{off}
5	1.22 ± 0.32	1.03 ± 0.62
30	7.0 ± 2.0	0.93 ± 0.60

release. This suggests that the physical step that mainly determines the k_{cat} value for TyrH is the release of the 4a-hydroxypterin, although the data presented here do not rule out a contribution of DOPA release to rate limitation. Another possibility is a rate-limiting conformational change associated with the release of 4a-hydroxypterin, since the viscosity data showed the presence of a rate-limiting conformational change in the case of $6MPH_4$ binding (see below).

The effect of changing solvent viscosity on the k_{cat} value confirms that turnover is substantially (~90%) limited by product release. Previous steady-state kinetic analyses with deuterated tyrosine established that the expected kinetic isotope effect upon hydroxylation is masked by a slower step (*9*, *20*, *42*); these results are consistent with product release being that step. The rate constants from the burst and linear phases of the chemical quench experiments can be used to calculate the expected viscosity effects on k_{cat} (*31*, *35*), yielding values of 0.95 at 5 °C and 0.85 at 30 °C. These are very similar to the experimental values obtained from the analysis of the steady-state data (Table 1).

The rapid reaction analyses were conducted at high concentrations of amino acid and $6MPH_4$ to avoid complications from binding steps. The effects of viscosity on steady-state k_{cat}/K_m values for tyrosine and $6MPH_4$ provide insight into these steps. The effect of increasing solvent viscosity on the k_{cat}/K_{tyr} value can be used to calculate the association rate constant (k_{on}) and the forward commitment (k_f/k_{off}) for tyrosine using eq 3 (*33*). Here, k_{on} and k_{off} are the rate constants for the association and dissociation of tyrosine, respectively, and k_f is the net rate constant for the subsequent step. The results (Table 3) indicate that the rate constant for tyrosine dissociation is comparable to the value of that net rate constant. Thus, tyrosine has a moderate forward commitment to catalysis. The first irreversible step in the TyrH reaction involves a change in the bond order of oxygen (*43*), consistent with either transfer of a single electron from tetrahydropterin to oxygen or concerted formation of the iron−peroxo−pterin intermediate (*16*). The value of k_f in Table 2 can be taken as a lower limit for the first irreversible step, placing a lower limit on the dissociation rate constant for tyrosine of 7−27 s^{-1}.

$$k_{cat}/K_m = \frac{k_{on}(\eta^0/\eta)}{1 + (k_{off}/k_f)(\eta^0/\eta)} \quad (3)$$

The effect of viscosity on the k_{cat}/K_m value for $6MPH_4$ is well above 1, the theoretical limit for a diffusion-limited event. Viscosity effects of >1 have previously been observed in systems where there is a conformational change accompanying binding of a substrate (*28*, *37*−*39*). In the case of TyrH, the movement of a mobile surface loop (amino acid residues 177−193) from a solvent-exposed position toward the active site is associated with $6MPH_4$ binding (*44*−*46*). An effect of the viscogen on this movement is a likely reason for the larger than expected effect of viscosity on the k_{cat}/K_m value for $6MPH_4$. The dependence of the effect of viscosity on the k_{cat}/K_m for $6MPH_4$ on the viscogen and temperature implies that there are differences in the interaction of sucrose and trehalose molecules with the flexible loop. Sucrose and trehalose have previously been reported to interact differently with water and proteins (*47*−*49*). Sucrose has been reported to make more hydrogen bonding interactions with proteins (*48*−*50*).

Overall, this study provides further insight into the mechanism of TyrH. Combining results from several kinetic analyses has allowed measurement of rate constants for individuals steps in the reaction. Turnover is limited by product release. Tyrosine has a moderate commitment to catalysis, while binding of the tetrahydropterin is coupled to protein motion.

REFERENCES

1. Fitzpatrick, P. F. (2003) Mechanism of aromatic amino acid hydroxylation. *Biochemistry 42*, 14083–14091.
2. Fitzpatrick, P. F. (2000) The aromatic amino acid hydroxylases. In Advances in Enzymology and Related Areas of Molecular Biology (Purich, D. L., Ed.) pp 235−294, John Wiley & Sons, Inc., New York.
3. Royo, M., Daubner, S. C., and Fitzpatrick, P. F. (2005) Effects of mutations in tyrosine hydroxylase associated with progressive dystonia on the activity and stability of the protein. *Proteins 58*, 14–21.
4. Zafeiriou, D. I., Willemsen, M. A., Verbeek, M. M., Vargiami, E., Ververi, A., and Wevers, R. (2009) Tyrosine hydroxylase deficiency with severe clinical course. *Mol. Genet. Metab. 97*, 18–20.
5. Que, L., Jr. (2000) One motif-many different reactions. *Nat. Struct. Biol. 7*, 182–184.
6. Goodwill, K. E., Sabatier, C., Marks, C., Raag, R., Fitzpatrick, P. F., and Stevens, R. C. (1997) Crystal structure of tyrosine hydroxylase at 2.3 Å and its implications for inherited neurodegenerative diseases. *Nat. Struct. Biol. 4*, 578–585.
7. Moran, G. R., Derecskei-Kovacs, A., Hillas, P. J., and Fitzpatrick, P. F. (2000) On the catalytic mechanism of tryptophan hydroxylase. *J. Am. Chem. Soc. 122*, 4535–4541.
8. Hillas, P. J., and Fitzpatrick, P. F. (1996) A mechanism for hydroxylation by tyrosine hydroxylase based on partitioning of substituted phenylalanines. *Biochemistry 35*, 6969–6975.
9. Frantom, P. A., and Fitzpatrick, P. F. (2003) Uncoupled forms of tyrosine hydroxylase unmask kinetic isotope effects on chemical steps. *J. Am. Chem. Soc. 125*, 16190–16191.
10. Pavon, J. A., and Fitzpatrick, P. F. (2005) Intrinsic isotope effects on benzylic hydroxylation by the aromatic amino acid hydroxylases: Evidence for hydrogen tunneling, coupled motion, and similar reactivities. *J. Am. Chem. Soc. 127*, 16414–16415.
11. Pavon, J. A., and Fitzpatrick, P. F. (2006) Insights into the catalytic mechanisms of phenylalanine and tryptophan hydroxylase from kinetic isotope effects on aromatic hydroxylation. *Biochemistry 45*, 11030–11037.
12. Panay, A. J., and Fitzpatrick, P. F. (2008) Kinetic Isotope Effects on Aromatic and Benzylic Hydroxylation by *Chromobacterium violaceum* Phenylalanine Hydroxylase as Probes of Chemical Mechanism and Reactivity. *Biochemistry 47*, 11118–11124.
13. Ellis, H. R., Daubner, S. C., and Fitzpatrick, P. F. (2000) Mutation of serine 395 of tyrosine hydroxylase decouples oxygen-oxygen bond cleavage and tyrosine hydroxylation. *Biochemistry 39*, 4174–4181.
14. Davis, M. D., and Kaufman, S. (1989) Evidence for the formation of the 4a-carbinolamine during the tyrosine-dependent oxidation of tetrahydrobiopterin by rat liver phenylalanine hydroxylase. *J. Biol. Chem. 264*, 8585–8596.
15. Eser, B. E., Barr, E. W., Frantom, P. A., Saleh, L., Bollinger, J. M., Jr., Krebs, C., and Fitzpatrick, P. F. (2007) Direct spectroscopic evidence for a high-spin Fe(IV) intermediate in tyrosine hydroxylase. *J. Am. Chem. Soc. 129*, 11334–11335.
16. Chow, M. S., Eser, B. E., Wilson, S. A., Hodgson, K. O., Hedman, B., Fitzpatrick, P. F., and Solomon, E. I. (2009) Spectroscopy and kinetics of wild-type and mutant tyrosine hydroxylase: Mechanistic insight into O_2 activation. *J. Am. Chem. Soc. 131*, 7685–7698.
17. Daubner, S. C., and Fitzpatrick, P. F. (1999) Site-directed mutants of charged residues in the active site of tyrosine hydroxylase. *Biochemistry 38*, 4448–4454.

18. Frantom, P. A., Seravalli, J., Ragsdale, S. W., and Fitzpatrick, P. F. (2006) Reduction and oxidation of the active site iron in tyrosine hydroxylase: Kinetics and specificity. *Biochemistry 45*, 2372–2379.
19. Ramsey, A. J., Hillas, P. J., and Fitzpatrick, P. F. (1996) Characterization of the active site iron in tyrosine hydroxylase: Redox states of the iron. *J. Biol. Chem. 271*, 24395–24400.
20. Fitzpatrick, P. F. (1991) The steady state kinetic mechanism of rat tyrosine hydroxylase. *Biochemistry 30*, 3658–3662.
21. Mathlouthi, M., and Genotelle, J. (1994) Rheological properties of sucrose solutions and suspensions. In Sucrose (Mathlouthi, M., and Reiser, P., Eds.) pp 126−154, Blackie Academic & Professional, New York.
22. Cheng, N. S. (2008) Formula for the viscosity of a glycerol-water mixture. *Ind. Eng. Chem. Res. 47*, 3285–3288.
23. Rampp, M., Buttersack, C., and Ludemann, H. D. (2000) c,T-dependence of the viscosity and the self-diffusion coefficients in some aqueous carbohydrate solutions. *Carbohydr. Res. 328*, 561–572.
24. Johnson, K. A., Simpson, Z. B., and Blom, T. (2009) Global Kinetic Explorer: A new computer program for dynamic simulation and fitting of kinetic data. *Anal. Biochem. 387*, 20–29.
25. Gampp, H., Maeder, M., Meyer, C. J., and Zuberbühler, A. D. (1985) Calculation of equilbrium constants from multiwavelength spectroscopic data. 1. Mathematical considerations. *Talanta 32*, 95–101.
26. Gampp, H., Maeder, M., Meyer, C. J., and Zuberbühler, A. D. (1985) Calculation of equilibrium constants from multiwavelength spectroscopic data. II. SPECFIT: Two user-friendly programs in BASIC and standard FORTRAN 77. *Talanta 32*, 257–264.
27. Johnson, K. A., Simpson, Z. B., and Blom, T. (2009) FitSpace Explorer: An algorithm to evaluate multidimensional parameter space in fitting kinetic data. *Anal. Biochem. 387*, 30–41.
28. McKay, G. A., and Wright, G. D. (1996) Catalytic Mechanism of Enterococcal Kanamycin Kinase (APH(3′)-IIIa): Viscosity, Thio, and Solvent Isotope Effects Support a Theorell-Chance Mechanism. *Biochemistry 35*, 8680–8685.
29. Kale, S., Ulas, G., Song, J., Brudvig, G. W., Furey, W., and Jordan, F. (2008) Efficient coupling of catalysis and dynamics in the E1 component of *Escherichia coli* pyruvate dehydrogenase multienzyme complex. *Proc. Natl. Acad. Sci. U.S.A. 105*, 1158–1163.
30. Caccuri, A. M., Antonini, G., Nicotra, M., Battistoni, A., Lo Bello, M., Board, P. G., Parker, M. W., and Ricci, G. (1997) Catalytic mechanism and role of hydroxyl residues in the active site of theta class glutathione S-transferases. Investigation of Ser-9 and Tyr-113 in a glutathione S-transferase from the Australian sheep blowfly *Lucilia cuprina*. *J. Biol. Chem. 272*, 29681–29686.
31. Cole, P. A., Burn, P., Takacs, B., and Walsh, C. T. (1994) Evaluation of the catalytic mechanism of recombinant human Csk (C-terminal Src kinase) using nucleotide analogs and viscosity effects. *J. Biol. Chem. 269*, 30880–30887.
32. Fitzpatrick, P. F., Kurtz, K. A., Denu, J. M., and Emanuele, J. J. (1997) Contrasting values of commitment factors measured from viscosity, pH, and kinetic isotope effects: evidence for slow conformational changes in the D-amino acid oxidase reaction. *Bioorg. Chem. 25*, 100–109.
33. Brouwer, A. C., and Kirsch, J. F. (1982) Investigation of diffusion-limited rates of chymotrypsin reactions by viscosity variation. *Biochemistry 21*, 1302–1307.
34. Johnson, W. W., Liu, S. X., Ji, X. H., Gilliland, G. L., and Armstrong, R. N. (1993) Tyrosine-115 Participates Both in Chemical and Physical Steps of the Catalytic Mechanism of a Glutathione-S-Transferase. *J. Biol. Chem. 268*, 11508–11511.
35. Adams, J. A., and Taylor, S. S. (1992) Energetic limits of phosphotransfer in the catalytic subunit of cAMP-dependent protein kinase as measured by viscosity experiments. *Biochemistry 31*, 8516–8522.
36. Wallick, D. E., Bloom, L. M., Gaffney, B. J., and Benkovic, S. J. (1984) Reductive activation of phenylalanine hydroxylase and its effect on the redox state of the non-heme iron. *Biochemistry 23*, 1295–1302.
37. Sampson, N. S., and Knowles, J. R. (1992) Segmental motion in catalysis: Investigation of a hydrogen bond critical for loop closure in the reaction of triosephosphate isomerase. *Biochemistry 31*, 8488–8494.
38. Simopoulos, T. T., and Jencks, W. P. (1994) Alkaline Phosphatase Is an Almost Perfect Enzyme. *Biochemistry 33*, 10375–10380.
39. Ricci, G., Caccuri, A. M., Lo Bello, M., Rosato, N., Mei, G., Nicotra, M., Chiessi, E., Mazzetti, A. P., and Federici, G. (1996) Structural flexibility modulates the activity of human glutathione transferase P1-1. Role of helix 2 flexibility in the catalytic mechanism. *J. Biol. Chem. 271*, 16187–16192.
40. Bailey, S. W., Rebrin, I., Boerth, S. R., and Ayling, J. E. (1995) Synthesis of 4a-hydroxytetrahydropterins and the mechanism of their nonenzymatic dehydration to quinoid dihydropterins. *J. Am. Chem. Soc. 117*, 10203–10211.
41. Köster, S., Stier, G., Ficner, R., Hölzer, M., Curtius, H.-C., Suck, D., and Ghisla, S. (1996) Location of the active site and proposed catalytic mechanism of pterin-4a-carbinolamine dehydratase. *Eur. J. Biochem. 241*, 858–864.
42. Fitzpatrick, P. F. (1991) Studies of the rate-limiting step in the tyrosine hydroxylase reaction: Alternate substrates, solvent isotope effects, and transition state analogs. *Biochemistry 30*, 6386–6391.
43. Francisco, W. A., Tian, G., Fitzpatrick, P. F., and Klinman, J. P. (1998) Oxygen-18 kinetic isotope effect studies of the tyrosine hydroxylase reaction: Evidence of rate limiting oxygen activation. *J. Am. Chem. Soc. 120*, 4057–4062.
44. Sura, G. R., Lasagna, M., Gawandi, V., Reinhart, G. D., and Fitzpatrick, P. F. (2006) Effects of ligands on the mobility of an active-site loop in tyrosine hydroxylase as monitored by fluorescence anisotropy. *Biochemistry 45*, 9632–9638.
45. Daubner, S. C., McGinnis, J. T., Gardner, M., Kroboth, S. L., Morris, A. R., and Fitzpatrick, P. F. (2006) A flexible loop in tyrosine hydroxylase controls coupling of amino acid hydroxylation to tetrahydropterin oxidation. *J. Mol. Biol. 359*, 299–307.
46. Wang, S., Sura, G. R., Dangott, L. J., and Fitzpatrick, P. F. (2009) Identification by hydrogen/deuterium exchange of structural changes in tyrosine hydroxylase associated with regulation. *Biochemistry 48*, 4972–4979.
47. Magazu, S., Maisano, G., Migliardo, P., Middendorf, H. D., and Villari, V. (1998) Hydration and transport properties of aqueous solutions of α-α-trehalose. *J. Chem. Phys. 109*, 1170–1174.
48. Cottone, G., Giuffrida, S., Ciccotti, G., and Cordone, L. (2005) Molecular dynamics simulation of sucrose- and trehalose-coated carboxy-myoglobin. *Proteins: Struct., Funct., Bioinf. 59*, 291–302.
49. Luzardo, M. d. C., Amalfa, F., Nunez, A. M., DÌaz, S., Biondi de Lopez, A. C., and Disalvo, E. A. (2000) Effect of Trehalose and Sucrose on the Hydration and Dipole Potential of Lipid Bilayers. *Biophys. J. 78*, 2452–2458.
50. Kawai, H., Sakurai, M., Inoue, Y., Chujo, R., and Kobayashi, S. (1992) Hydration of oligosaccharides: Anomalous hydration ability of trehalose. *Cryobiology 29*, 599–606.